An Electron-Accepting aza-BODIPY-Based Donor-Acceptor-Donor Architecture for Bright NIR Emission

Kage, Yuto
Department of Chemistry and Biochemistry Graduate School of Engineering, Kyushu University

Kang, Seongsoo
Spectroscopy Laboratory for Functional π-Electronic Systems Department of Chemistry Yonsei University

Mori, Shigeki
Advanced Research Support Center (ADRES) Ehime University

Mamada, Masashi
Department of Chemistry and Biochemistry Graduate School of Engineering, Kyushu University

他

出版情報：Chemistry - A European Journal. 27 (16), pp.5259-5267, 2021-03-18. Wiley
バージョン：

An Electron-Accepting aza-BODIPY-Based Donor–Acceptor–Donor Architecture for Bright NIR Emission

Yuto Kage,[a] Seongsoo Kang,[b] Shigeki Mori,[c] Masashi Mamada,*[a,d] Chihaya Adachi,[a,d,e] Dongho Kim,*[b] Hiroyuki Furuta,*[a,f] and Soji Shimizu*[a,f]

[a] Dr. Y. Kage, Dr. M. Mamada, Prof. Dr. C. Adachi, Prof. Dr. H. Furuta, Prof. Dr. S. Shimizu
Department of Chemistry and Biochemistry, Graduate School of Engineering, Kyushu University
Fukuoka 819-0395 (Japan)
E-mail: hfuruta@cstf.kyushu-u.ac.jp, ssoji@cstf.kyushu-u.ac.jp

[b] S. Kang, Prof. Dr. D. Kim
Spectroscopy Laboratory for Functional π-Electronic Systems, Department of Chemistry, Yonsei University
Seoul 120-749 (Korea)
E-mail: dongho@yonsei.ac.kr

[c] Dr. S. Mori
Advanced Research Support Center (ADRES), Ehime University
Matsuyama 790-8577 (Japan)

[d] Dr. M. Mamada, Prof. Dr. C. Adachi
Center for Organic Photonics and Electronics Research (OPERA), Kyushu University
Fukuoka 819-0395 (Japan)
E-mail: mamada@opera.kyushu-u.ac.jp

[e] Prof. Dr. C. Adachi
International Institute for Carbon Neutral Energy Research (WPI-I2CNER), Kyushu University
Fukuoka 819-0395 (Japan)

[f] Prof. Dr. H. Furuta, Prof. Dr. S. Shimizu
Center for Molecular Systems (CMS), Kyushu University
Fukuoka 819-0395 (Japan)

Supporting information for this article is given via a link at the end of the document.

Abstract: A bright near-infrared (NIR) fluorescent molecule was developed based on the donor–acceptor (D–A) approach using an aza-BODIPY analog called pyrrolopyrrole aza-BODIPY (PPAB) as an electron-accepting chromophore. Directly introducing electron-donating triphenylamine (TPA) to elaborate a D–A–D structure caused redshifts of absorption and emission of PPAB into the NIR region with the enhanced fluorescence brightness up to 0.5×10^5 $M^{-1}cm^{-1}$, whereas inserting a phenylene linker between the TPA donor and PPAB acceptor induced solvatochromic behaviors in emission. The transient absorption spectra and theoretical calculations revealed the presence of a highly emissive hybridized locally excited and charge-transfer state in the former case and the contribution of the dark charge-separated state to the excited state in the latter case. The bright D–A–D PPAB as a novel emitter resulted in a NIR electroluminescence with a high external quantum efficiency of 3.7% and a low amplified spontaneous emission threshold of ca. 80 $\mu J\ cm^{-2}$, indicating the high potential for NIR optoelectronic applications.

Introduction

Organic chromophores exhibiting intense absorption and emission in the near infrared (NIR) region are exceedingly important owing to the growing demand to harness the NIR light for a wide range of applications,[1] such as organic photovoltaics (OPVs),[2,3] organic light emitting diodes (OLEDs),[4] telecommunications,[5,6] bioimaging,[7,8] and photothermal and photodynamic therapies.[9,10] Aza-boron dipyrromethene (aza-BODIPY)[11–14] is one of the potential chromophores to target the NIR region by structural modification owing to its intense emission in the far-red region at around 670 nm.[11a,15,16] Recently, we have developed a dimeric aza-BODIPY analog called pyrrolopyrrole aza-BODIPY (PPAB)[17] as a novel NIR chromophore. Because of its facile synthesis from commercially available diketopyrrolopyrrole (DPP) and readily tunable absorption and emission wavelengths by changing heteroaromatic ring units and aryl substituents in the structure,[17,18] PPAB has been applied in various research fields: electrochemiluminescence,[19] OPV,[20] aggregation-induced emission,[21] two-photon absorption,[22] photoacoustic imaging,[23,24] and photothermal therapy.[24] Despite the expectation of PPAB as a potential NIR chromophore toward biomedical and optoelectronic applications, its fluorescence brightness,[25] a simple parameter to make meaningful comparison between different kinds of fluorescent molecules, which is defined by the product of the molar absorption coefficient and the fluorescence quantum yield ($\varepsilon_{Abs} \times \Phi_{Fl}$), decreases as the absorption shifts to the NIR region (Figure 1). A similar trend is seen for conventional NIR fluorescent molecules, such as Cyx series.[26] This trend is explained in terms of the energy gap law,[27] which specifies that nonradiative decay processes are accelerated by vibrational relaxation due to the enhanced overlap of the vibrational levels of the lowest singlet excited state (S_1) and the ground state (S_0), lying with narrow energy gaps.

Recently, NIR fluorescent molecules with high Φ_{Fl} were developed by introducing electron-donors to electron-accepting fluorophores such as benzobis(1,2,5-thiadiazole) (BBTD).[28–30] The resulting donor–acceptor–donor (D–A–D) structure can mitigate fluorescence quenching dictated by the energy gap law owing to the contribution of the intramolecular charge transfer (ICT) in the excited state. However, insufficiently enhanced ICT due to unbalanced D–A interactions or twisting of D–A units can facilitate fluorescence quenching due to the formation of a dark charge-separated (CS) state. In addition, an enhanced ICT nature in the absorption may also decrease ε_{Abs} in a quadrupolar structure. Therefore, to attain high fluorescence brightness in the

NIR region, it is primarily important to tune donor interactions to the core electron-accepting chromophore by optimizing D–A combinations and by adjusting D–A distances and twisting angles.

In the plots of fluorescence brightness as a function of emission wavelength, two trends can be seen for the fluorescence brightness of PPABs (Figure 1): 1. except for **Ph-4**, PPABs with phenyl substituents on the pyrrolopyrrole moiety and different kinds of heteroaromatic ring units (**Ph-x** series) are positioned in the higher fluorescence brightness range than those with thienyl and oligothienyl substituents (**Th-x** series); 2. in the **Th-x** series, upon elongation of the oligothienyl substituents from **Th-1** to **Th-2** and **Th-3**, the fluorescence brightness increases despite the redshifts of the emission wavelength. The former trend is ascribed to the inherently higher Φ_{Fl} of the **Ph-x** series than that of the **Th-x** series owing to the hindered rotation of the phenyl substituents compared with the thienyl substituents. The rigid structures of the **Ph-x** series reduce nonradiative decay processes. The latter trend can be rationalized by considering a D–A–D architecture for the **Th-x** series, in which PPAB functions as an electron-accepting chromophore.[20] The high ε_{Abs} of the **Th-x** series also indicates that introduction of donor units to these positions is suitable for maintaining a high ε_{Abs} of PPAB owing to the resulting *pseudo*-quadrupolar structure.[31]

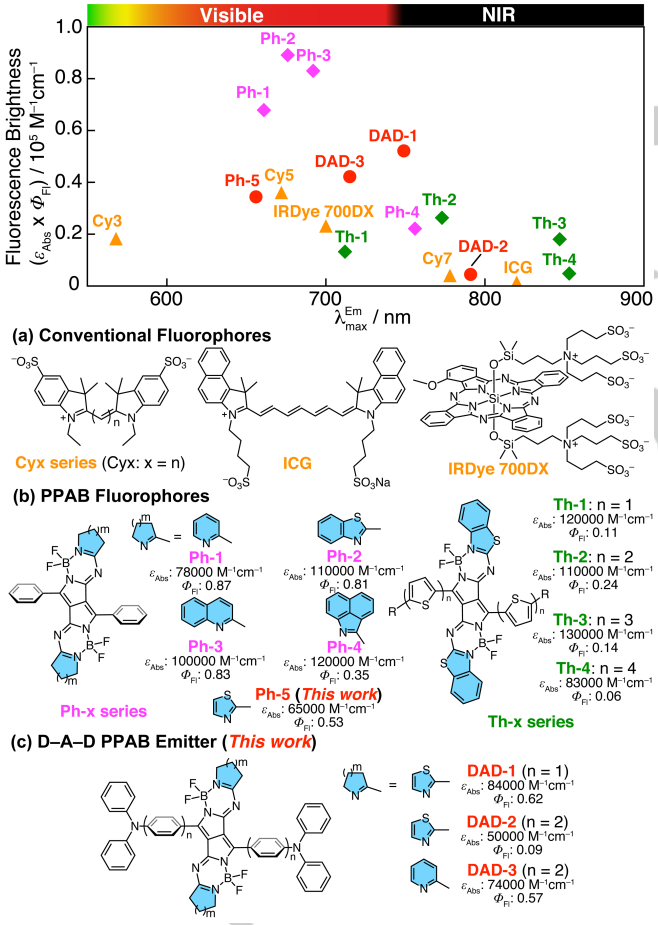

Figure 1. Plots of fluorescence brightness ($\varepsilon_{Abs} \times \Phi_{Fl}$ / $M^{-1}cm^{-1}$) vs wavelength of the emission maximum (λ_{max}^{Em}). Fluorescence brightness data of Cyx series, ICG, IRDye 700DX, and PPABs (**Ph-x** and **Th-x** series) were adopted from literatures. [17,18,26,32,33] Substituents are omitted for the structures in (b) and (c).

Considering the above-mentioned trends, here we elaborated a D–A–D PPAB as a bright NIR emitter based on the structure of the **Ph-x** series (Figure 1c). To enhance the electron-accepting nature of PPAB, thiazole rings were introduced as a heteroaromatic ring unit, whereas triphenylamine (TPA) was used as a donor unit. The relationship between D–A interactions and emission properties was investigated by inserting a phenylene spacer. The fluorescence brightness up to 5.2×10^4 $M^{-1}cm^{-1}$ in the NIR region was ultimately achieved for **DAD-1** bearing directly linked TPA units. Inserting a phenylene spacer induced solvent-polarity-dependent emission behaviors of **DAD-2** and **DAD-3** featured by the intense locally-excited (LE) emission in apolar solvents and the broad ICT emission with a significant decrease of the Φ_{Fl} in polar solvents. Owing to the high fluorescence brightness and radiative rate constant in the NIR region, **DAD-1** exhibited electroluminescence (EL) at 760 nm with a high external quantum efficiency of 3.7% and a low amplified spontaneous emission (ASE) threshold of ca. 80 μJ cm^{-2}.

Results and Discussion

PPAB with phenyl (**3**) and *p*-bromophenyl (**4**) substituents were synthesized by a Schiff base forming reaction of the corresponding DPPs (**1** and **2**) and 2-amino-5-nonylthiazole in the presence of $TiCl_4$ and triethylamine and a subsequent boron complexation (Scheme 1). A Buchwald-Hartwig amination reaction of **4** afforded a D–A–D PPAB bearing TPA groups (**DAD-1**), while Suzuki-Miyaura cross coupling reaction with *p*-diphenylaminophenylboronic acid provided a D–A–D PPAB with a phenylene spacer (**DAD-2**). To reveal the role of the thiazole groups as an electron-deficient unit, a pyridine-substituted counterpart (**DAD-3**) was also synthesized from the corresponding PPAB (**5**). All compounds were fully characterized by ^1H and ^{13}C NMR spectroscopy, high-resolution mass spectrometry, and X-ray single crystal diffraction analysis (Figures 2 and S1–S12).

A degree of conjugation between the TPA donors and the PPAB acceptor was estimated from the C–N bond lengths of the TPA units (L_{TPA}) and torsional twisting of the TPA units from the mean plane of the PPAB moiety, which was estimated from the dihedral angles (θ_{TPA}, $\theta_{PPAB\text{-}Ph}$, and $\theta_{Ph\text{-}Ph'}$) (Figure 2). Because of the absence of a phenylene spacer, the overall torsional twisting in **DAD-1** is moderate compared with **DAD-2** and **DAD-3**. In addition, a slightly shorter L_{TPA} of **DAD-1** (1.392(6) Å) implies weak but viable conjugation between the donors and acceptor. In contrast, the L_{TPA} of **DAD-2** and **DAD-3** in a normal C(sp^2)–N single bond distance (1.420(3) Å for **DAD-2** and 1.426(3) Å for **DAD-3**) indicates a minor degree of conjugation.

In chloroform, **DAD-1–3** exhibit similar steady-state absorption spectra to reference compound **3** (Figure 3a). The absorption spectra in the far-red/NIR regions show redshifts in order of **3** (636 nm), **DAD-2** (666 nm), **DAD-3** (683 nm), and **DAD-1** (705 nm). In addition to the bathochromic shifts, the broad absorption spectra were observed in the visible region (450–600 nm) (λ_{max}: 528 nm for **DAD-1**, 553 nm for **DAD-2**, and 525 nm for **DAD-3**). As shown in Figure S13 and Table 1, minor solvatochromic behaviors of the steady-state absorption spectra reveal an apolar nature of D–A–D PPABs in the ground state.

In contrast, the notable solvatochromic response depending on the D–A–D spacer lengths and heteroaromatic ring units

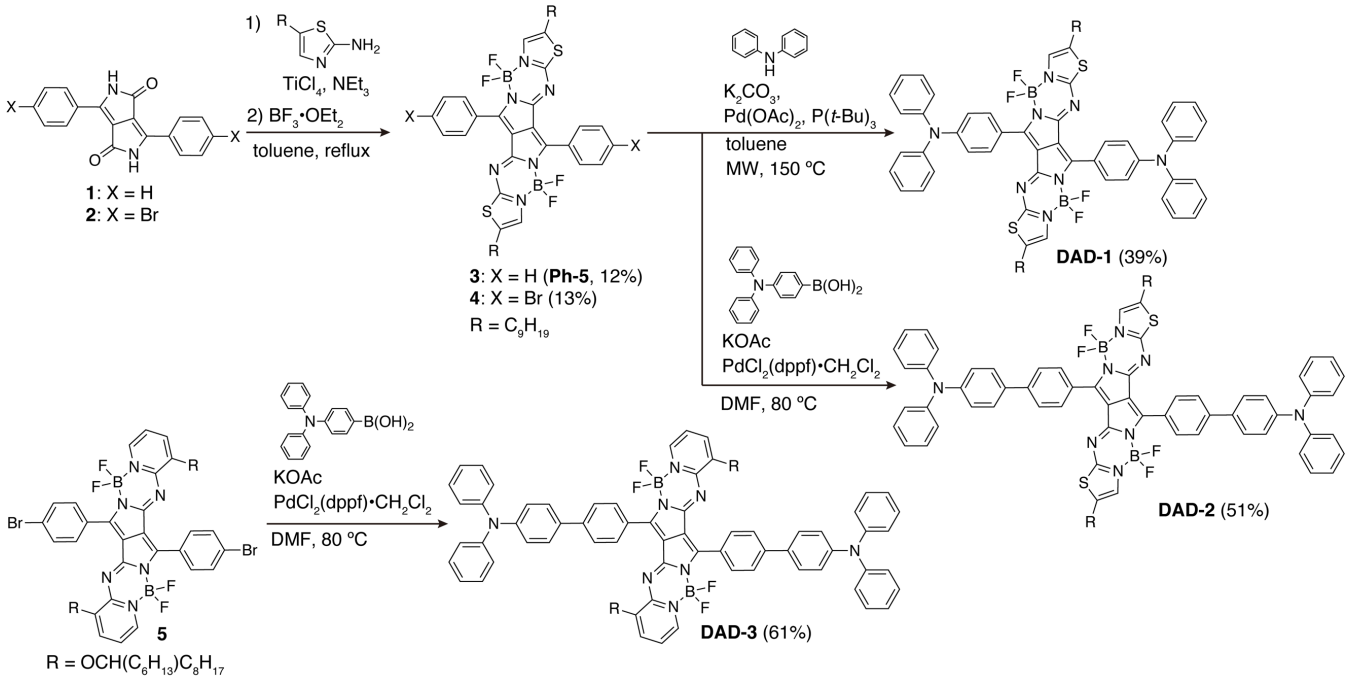

Scheme 1. Synthesis of a series of D–A–D PPABs.

were observed in the fluorescence spectra (Figures 3b and S14, and Table 1). In chloroform, **3**, **DAD-1**, and **DAD-3** exhibit a sharp emission, which is a mirror image of the far-red/NIR absorption. The fluorescence lifetimes (τ_{Fl}) of **DAD-1** (5.2 ns) and **DAD-3** (4.4 ns) are similar to that of **3** (3.4 ns), identifying their origin as a PPAB-centered LE emission (Figures S15 and Table 1). Despite the redshifts of the emission spectra, the Φ_{Fl} increases in order of **3** (0.53), **DAD-3** (0.57), and **DAD-1** (0.62). In contrast, in chloroform, **DAD-2** exhibits broad and structureless fluorescence spectrum featured by the large Stokes shift, small Φ_{Fl} of 0.09, and shortened fluorescence lifetime of 0.98 ns. In toluene, **DAD-2** shows the sharp fluorescence spectrum with similar photophysical properties (Φ_{Fl}: 0.57 and τ_{Fl}: 4.4 ns) to the other D–A–D PPABs. In polar benzonitrile solutions, the fluorescence of all D–A–D PPABs is virtually quenched, and the fluorescence lifetimes are one-to-two order shorter than those in chloroform and toluene (0.02–0.65 ns) (Table 1). Considering that in benzonitrile, **3** exhibits almost identical fluorescence spectrum with similar photophysical properties to those in chloroform and toluene, the observed solvatochromic behaviors can be ascribed to a polar nature of the D–A–D PPABs in the excited state, implying contribution of the ICT to the S_1 state.

Despite the redshift of the emission wavelength from **3** to **DAD-1**, the fluorescence brightness is inversely enhanced (**3**: 3.4 $\times$ 10^4 $M^{-1}cm^{-1}$ and **DAD-1**: 5.2 $\times$ 10^4 $M^{-1}cm^{-1}$), breaking the energy gap law. In fact, **DAD-1** is significantly bright compared with conventional fluorophores in the corresponding region, such as Cy7,[26] indocyanine green (ICG),[32] and IRDye700DX[33] (Figure 1a). The observed enhancement of the fluorescence brightness is ascribed to the large ε_{Abs} in addition to the high Φ_{Fl}. The large ε_{Abs} of **DAD-1** (8.4 $\times$ 10^4 $M^{-1}cm^{-1}$) is caused by the enhanced oscillator strength due to the D–A–D structure. The time-dependent (TD) DFT calculations at the ωB97XD/6-31G(d,p) level gave insights into the high ε_{Abs} and Φ_{Fl} of **DAD-1**. Optimized structures in the S_0 and S_1 states are broadly similar to the X-ray single crystal structures (Figures S16–S19). The $S_0 \rightarrow S_1$ transition mainly comprises a HOMO $\rightarrow$ LUMO transition for **3** and **DAD-1** and HOMO $\rightarrow$ LUMO and HOMO–2 $\rightarrow$ LUMO transitions for **DAD-2** and **DAD-3** (Tables 2 and S1–S4). The redshifts of this transition from **3** are mainly caused by the destabilization of the HOMO (Figures 4 and S20). The calculated oscillator strength (*f*) of the $S_0 \rightarrow S_1$ transition increases from **3** (*f* = 0.71 (λ = 515 nm)) to **DAD-1** (*f* = 0.85 (λ = 557 nm)) because the delocalized HOMO of **DAD-1** along the D–A–D axis may enhance the transition dipole moment (Figure S21). Although the TDDFT calculations also predicted similarly large oscillator strengths for **DAD-2** (*f* = 0.82, λ = 533 nm) and **DAD-3** (*f* = 0.88, λ = 527 nm), the ε_{Abs} of **DAD-2** (5.0 $\times$ 10^4 $M^{-1}cm^{-1}$) and **DAD-3** (7.4 $\times$ 10^4 $M^{-1}cm^{-1}$) are rather smaller than that of **DAD-1** and slightly larger than that of **3** (6.5 $\times$ 10^4 $M^{-1}cm^{-1}$). From the fact that the ε_{Abs} decreases with respect to the energy difference between the far-red/NIR absorption ($S_0 \rightarrow S_1$ transition) and the broad absorption in the range of 450–600 nm (**DAD-1**: 4.8 $\times$ 10^3 cm^{-1} > **DAD-3**: 4.4 $\times$ 10^3 cm^{-1} > **DAD-2**: 3.1 $\times$ 10^3 cm^{-1}), this can be rationalized considering the ICT nature for the broad bands and their intensity borrowing from the $S_0 \rightarrow S_1$ transition. The natural transition orbital (NTO) calculations on the first three or four transitions (Figures S22–S25) revealed enhanced ICT natures for the higher energy transitions ($S_0 \rightarrow S_3$ transition for **DAD-1** and **DAD-2**, and $S_0 \rightarrow S_4$ transition for **DAD-3**). In these transitions, the hole densities are delocalized on the whole molecule, whereas the electron densities are localized on the PPAB moiety. Owing to the sufficient separation of the far-red/NIR absorption from the broad ICT band, it can be concluded that the directly TPA-attached D–A–D structure in **DAD-1** is ideal for attaining high ε_{Abs}. This structure also benefits in retaining the high Φ_{Fl}. The NTO calculations on emission ($S_1 \rightarrow S_0$ detransition)

of **DAD-1** revealed delocalization of both electron and hole on the whole molecule, exhibiting hybridized LE and CT (HLCT) nature (Figures S27). Because of the large transition moment from the LE state and enhanced ICT nature, which can mitigate the vibrational nonradiative relaxation, the HLCT is a highly emissive state.[34] In contrast, the localized electron and hole on the PPAB moiety in the NTOs of **DAD-2** and **DAD-3** indicated the LE nature for the emission, which agrees with the fluorescence spectra of **DAD-2** in toluene and **DAD-3** in toluene and chloroform (Figures S26, S28, and S29).

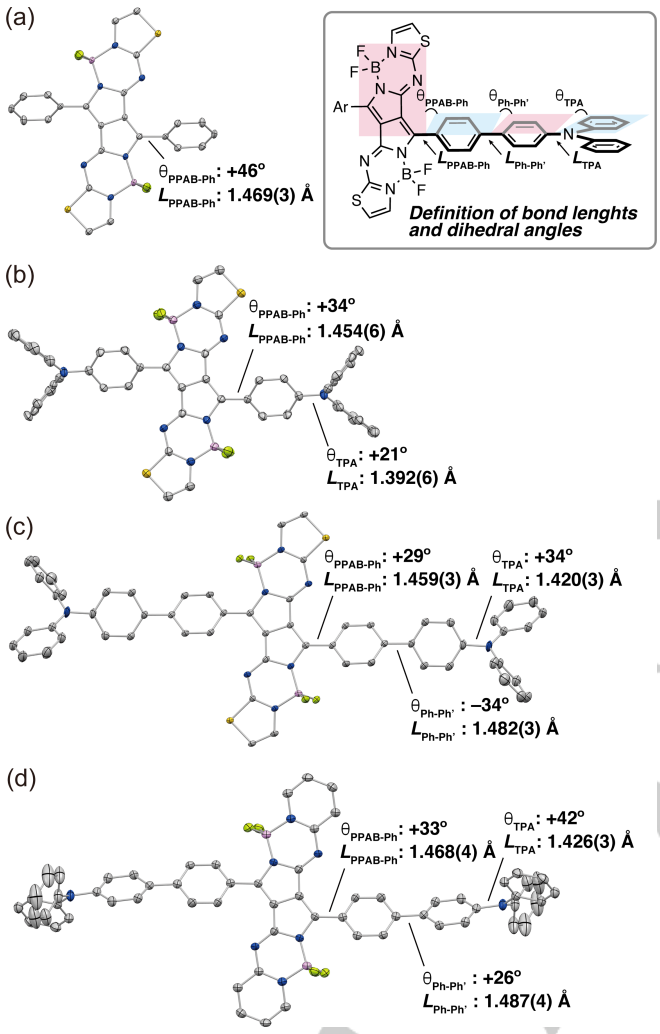

Figure 2. X-ray single crystal structures of (a) **3**, (b) **DAD-1**, (c) **DAD-2**, and (d) **DAD-3**. Substituents and hydrogen atoms are omitted for clarity. The thermal ellipsoids are scaled to the 50% probability. Inset indicates definition of bond lengths and dihedral angles. θ is plus for clockwise rotation and minus for counterclockwise rotation when viewing from the PPAB moiety to the TPA moiety.

To give an in-depth insight into the fluorescence quenching of D–A–D PPAB in polar media, femtosecond transient absorption (TA) spectra were measured. In toluene, the TA spectra of all compounds exhibit a broad ground-state bleaching (GSB) and stimulated emission (SE) features corresponding to the steady-state absorption and fluorescence spectra, respectively, with double exponential decay components with fast (4–20 ps) and slow (3–5 ns) time constants (Figures 5a and S30–S32). The fast

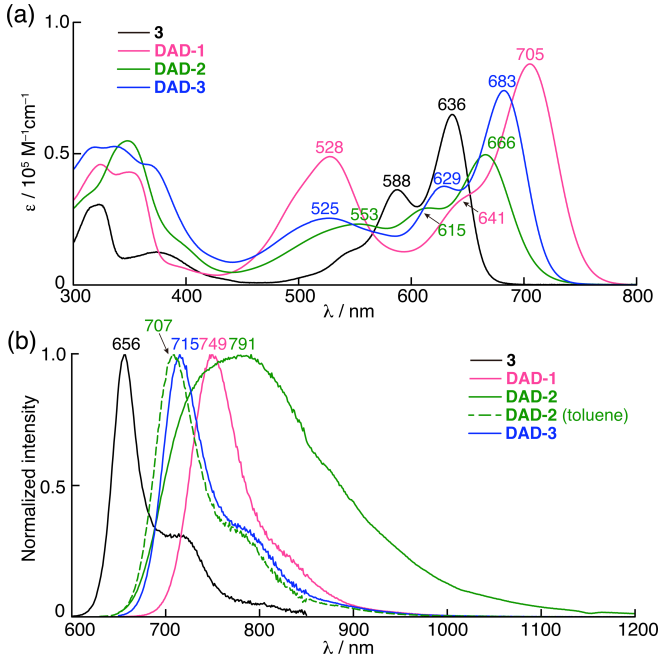

Figure 3. (a) UV/vis/NIR absorption and (b) fluorescence spectra of **3** and **DAD-1–3** in chloroform. The fluorescence spectrum of **DAD-2** in toluene is shown by a dashed green line.

Table 1. Photophysical properties of **3** and **DAD-1–3**.

Compd	Solvent[a]	λ_{max}^{Abs} [b] [nm]	λ_{max}^{Em} [c] [nm]	Φ_{Fl}[d]	τ_{Fl}[e] [ns]	k_r[f] [10^8 s^{-1}]	k_{nr}[f] [10^8 s^{-1}]
3	Tol	642	659	0.48	3.7	1.3	1.4
	CF	636	656	0.42	3.4	1.2	1.7
	BCN	645	666	0.26	2.2	1.2	3.4
DAD-1	Tol	704	741	0.67	5.0	1.3	0.66
	CF	705	749	0.65	5.2	1.3	0.67
	BCN	710	763	0.08	0.65	1.2	14
DAD-2	Tol	670	707	0.57	4.4	1.3	0.97
	CF	666	791	0.06	0.98	0.61	9.6
	BCN	675	712	–	0.02	–	–
DAD-3	Tol	688	712	0.49	4.5	1.1	1.1
	CF	683	715	0.55	4.4	1.3	1.0
	BCN	694	723	< 0.01	0.07	1.4	140

[a] BCN, CF, and Tol denote benzonitrile, chloroform, and toluene, respectively. [b] Absorption maximum. [c] Emission maximum. [d] Fluorescence quantum yield. [e] Fluorescence lifetime. [f] k_r and k_{nr} denote radiative and nonradiative decay constants, respectively: $k_r = \Phi_{Fl}/\tau_{Fl}$ and $k_{nr} = (1-\Phi_{Fl})/\tau_{Fl}$.

decay components are assigned as vibrational relaxation or structural reordering processes, whereas the slow ones are ascribed to decay process from the S_1 state because the slow components correspond to the fluorescence lifetimes (Table 1).

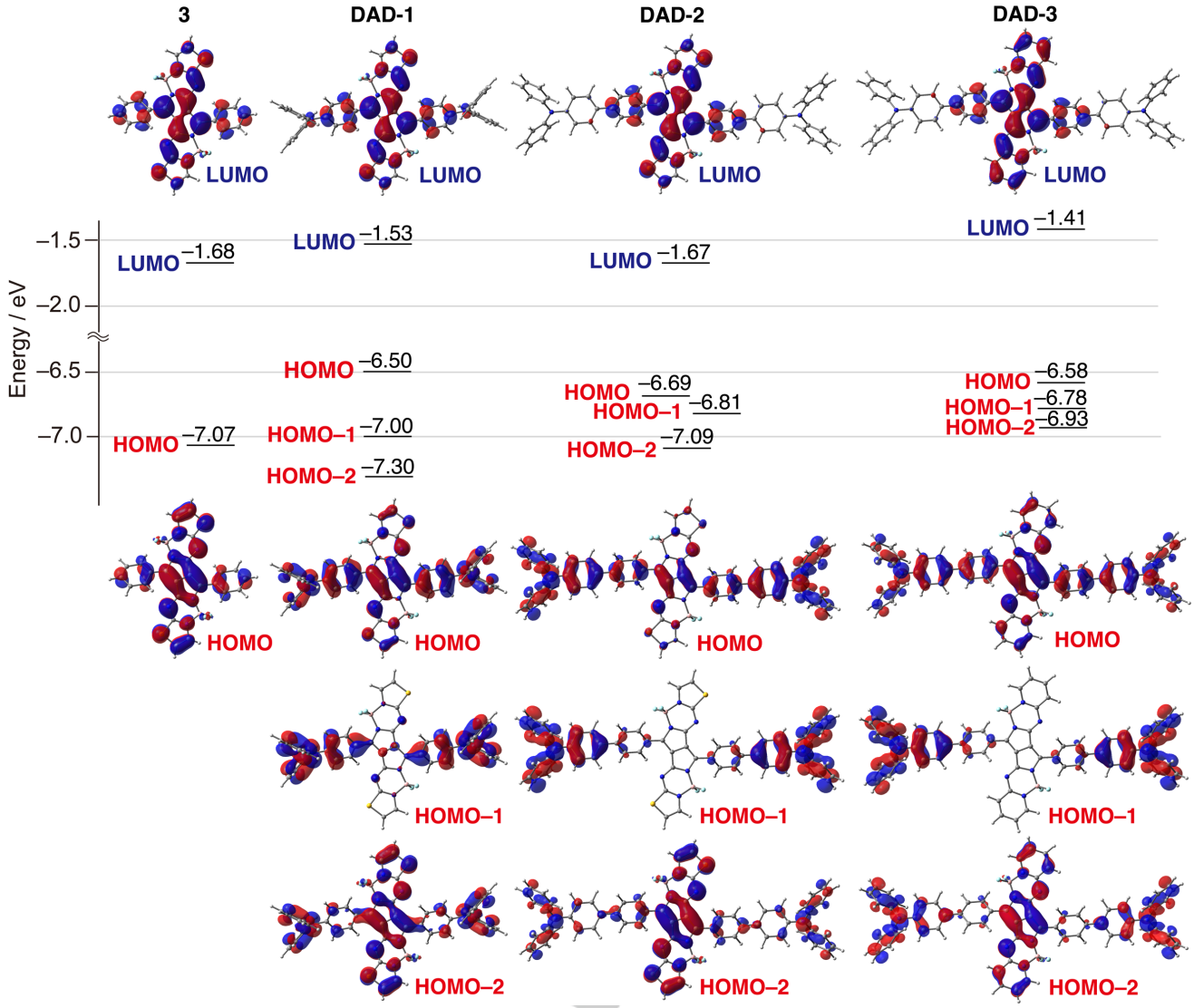

Figure 4. Partial frontier MO diagram of **3** and **DAD-1**–**3** at the ωB97XD/6-31G(d,p) level. A detailed MO diagram is shown in Figure S20.

Table 2. $S_0 \rightarrow S_1$ transition wavelengths, oscillator strengths, and major contributions of **3** and **DAD-1**–**3** calculated by the TDDFT method at the ωB97XD/6-31G(d,p) level.

Compd	λ[a]	*f* [b]	Major contributions (weight%)[c]
3	515	0.71	H→L (97%)
DAD-1	557	0.85	H→L (86%)
DAD-2	533	0.82	H-2→L (53%), H→L (43%)
DAD-3	527	0.88	H-2→L (31%), H→L (65%)

[a] Wavelength [nm]. [b] Oscillator strength. [c] H and L denote the HOMO and LUMO, respectively.

In chloroform, **3**, **DAD-1**, and **DAD-3** exhibit similar TA spectra to those in toluene (Figure 5d–f). In contrast, the TA spectra of **DAD-2** in chloroform show spectral evolution in the region of 500–780 nm due to the transition from the S_1 state to the ICT state (Figure 5b). In particular, the band in the range of 700–750 nm region reflects the excited-state absorption (ESA) of triphenylamine radical cation,[35] indicating the photoinduced electron transfer (PET) from the TPA moieties to the PPAB core. The excited-state dynamics is fitted with biexponential decay with time constants of 11.8 and 885 ps. The fast and slow components are, therefore, ascribed to the charge separation process and the decay process of the CS state, respectively.

In benzonitrile, the TA spectra of **DAD-3** also exhibit the ESA features of triphenylamine radical cation in the range of 700–750 nm as with **DAD-2** (Figures 5c and S32). The facilitated excited-state dynamics as compared with that in chloroform imply the accelerated charge separation and recombination processes by the enhanced CT character in polar media. In contrast, the TA spectra of **DAD-1** do not show the ESA features corresponding to triphenylamine radical cation in benzonitrile despite the faster excited-state dynamics with time constants of 6.1 and 600 ps than those in nonpolar media. These results imply that **DAD-1**

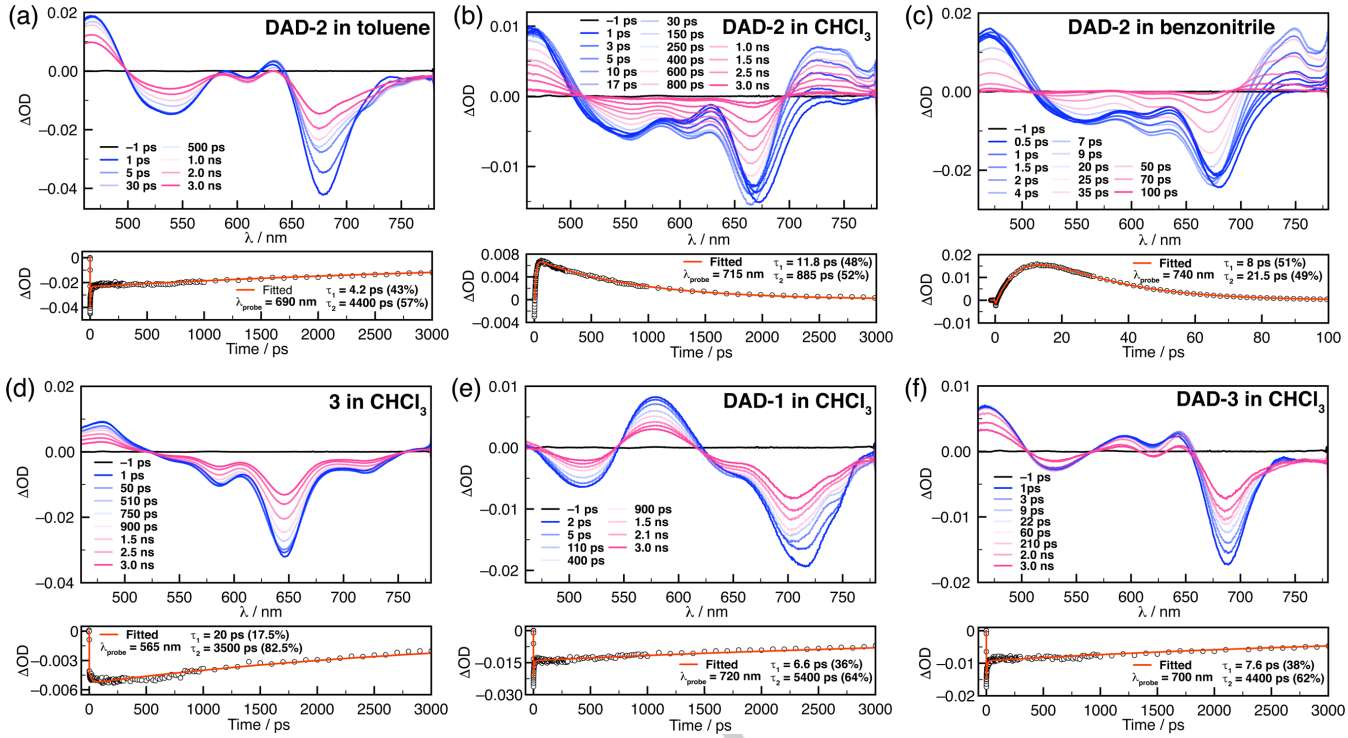

Figure 5. Transient absorption spectra (top) and decay profiles (bottom) of **DAD-2** in (a) toluene, (b) chloroform, and (c) benzonitrile with photo-excitation at 650 nm and transient absorption spectra of (d) **3**, (e) **DAD-1**, and (f) **DAD-3** in chloroform with photo-excitation at 650 nm. Transient absorption spectra and decay profiles in other solvents were reported in the Supporting Information (Figures S30–S32).

goes through the HLCT state, but not through the CS state in the excited state dynamics.

The difference in the excited-state dynamics between **DAD-1** and other D–A–D PPABs can be explained in terms of the rotational flexibility of the TAP donor units along the D–A–D axis. The moderate twisting in the excited state as shown in the S_1 optimized structure (Figure S17) can facilitate **DAD-1** to take the HLCT state. In contrast, the observed CS state for **DAD-2** and **DAD-3** implies the enhanced twisting of donor and acceptor units in the excited state in polar media compared with their S_1 optimized structures (Figures S18–S19). This may hinder the charge recombination process to render the excited state to be a dark CS state. Because the excited state dynamics depend on the molecular structures and D–A interactions, the solvatochromic behaviors in the fluorescence spectra are slightly different between **DAD-2** and **DAD-3**. The broad fluorescence spectra of **DAD-2** in chloroform and benzonitrile can be ascribed to the emission from the CS state, which borrows intensity from the LE state.[36] On the other hand, the sharp fluorescence spectrum of **DAD-3** in benzonitrile, which is similar to those in toluene and chloroform, implies major contribution of the LE state for the emission, whereas the fluoresce quenching in benzonitrile is mainly governed by the dark CS state.

The observed excited state dynamics of **DAD-2** and **DAD-3** were also supported by the calculated charge separation energy (ΔG_{CS}) using the Rehm-Weller equation (eq. S1, Figures S33–S35, and Table S5).[37] The negative ΔG_{CS} values of –0.31 eV for **DAD-2** and –0.33 eV for **DAD-3** in benzonitrile indicate facile internal conversion from the LE state to the CS state. In contrast, the calculated up-hill process from the LE state to the CS state in toluene with positive ΔG_{CS} values of 0.24 eV for **DAD-2** and 0.27 eV for **DAD-3** agree with the observed emission from the LE state. Small negative ΔG_{CS} values for both **DAD-2** (–0.08 eV) and **DAD-3** (–0.04 eV) in chloroform are contradictory to the observed differences in the fluorescence and TA spectra. This is probably due to the difficulty in estimating such subtle energy differences between the LE and CS states in chloroform by the Rehm-Weller equation because of its approximate treatment. From the observed fluorescence and TA spectra, it can be concluded that in chloroform, the CS state of **DAD-2** is more stable than the LE state, whereas the LE state of **DAD-3** is dominant compared with the CS state. This ensures that the heteroaromatic ring units affect the electron-accepting nature of the PPAB moiety.

EL properties of **DAD-1** as a bright NIR emitter were investigated using OLEDs based on a thermally activated delayed fluorescence (TADF)-assisted fluorescence (TAF) system. In the TAF system, Förster-type energy transfer (FRET) from the TADF sensitizer to the fluorescence emitter enables high external quantum efficiencies (EQEs) and tunable emission colors.[38]

Poly-(3,4-ethylenedioxythiophene):poly(styrenesulfonic acid) (PEDOT:PSS), 2,4,6-tris(biphenyl-3-yl)-1,3,5-triazine (T2T) and 2,7-bis(2,20-bipyridine-5-yl)triphenylene (BPy-TP2), and 8-quinolinato lithium (Liq) and aluminum (Al) were used as a hole injection material, electron transport materials, and cathode materials, respectively (Figure S36). The device structure of the **DAD-1** OLEDs was ITO/PEDOT:PSS/emissive layer (45 nm)/T2T (10 nm)/BPy-TP2 (50 nm)/Liq (2 nm)/Al. The emissive layer (EML) consisted of **DAD-1**, 7,10-bis[4-(diphenylamino)phenyl]-2,3-dicyanopyrazinophenanthrene (TPA-DCPP) as a TADF assistant material,[39] and 4,4'-bis(carbazol-9-yl)biphenyl (CBP) as a host

material (**DAD-1**: x wt%, TPA-DCPP: y wt%, and CBP: $100 - x - y$ wt%, where x = 0.5, 1.0, and 1.5 and y = 20, 35, and 50). The photoluminescence (PL) properties of each EML were evaluated (Figure 6).

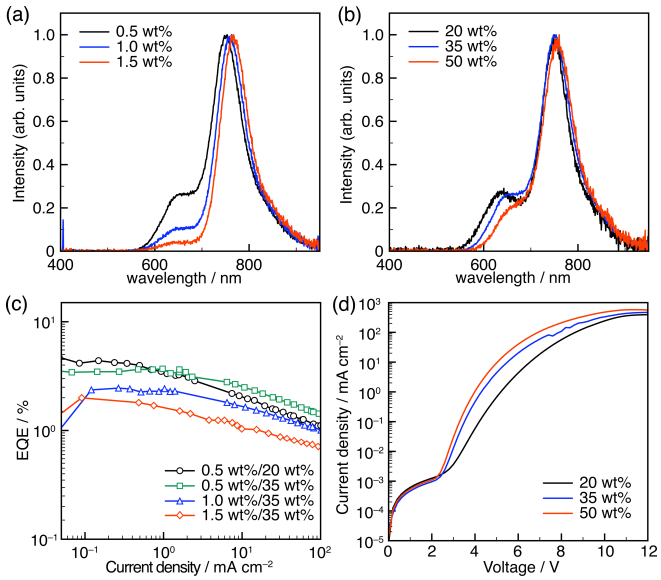

Figure 6. EL spectra of **DAD-1** OLEDs (a) with various doping concentrations (0.5, 1.0, and 1.5 wt%) and the fixed TPA-DCPP concentration of 20 wt% and (b) with various TPA-DCPP concentrations (20, 35, and 50 wt%) and the fixed doping concentration of 0.5 wt%. (c) EQE as a function of current density. (d) *J*–*V* characteristics with various TPA-DCPP concentrations (20, 35, and 50 wt%) and the fixed doping concentration of 1.0 wt%.

The EL spectra of all devices exhibited sharp emission with small full width at half maximum (FWHM) of 0.17 eV, which is a summation of a narrow NIR emission from **DAD-1** at ca. 760 nm and a small shoulder around 640 nm due to the TADF from TPA-DCPP. As the emitter concentrations were increased from 0.5 wt% to 1.5 wt%, the shoulder emission decreased due to efficient FRET from TPA-DCPP to **DAD-1** (Figure 6a). However, the external quantum efficiencies (EQE) decreased because the NIR emitters with a narrow energy gap tend act as a carrier trap (Figure 6c). A decrease of the shoulder emission was also observed due to the concentration quenching when the concentrations of TPA-DCPP were increased (Figure 6b). The driving voltage in the current density–voltage (*J*–*V*) curves were decreased with increasing the TPA-DCPP concentrations as observed in the previous report (Figure 6d),[38] whereas **DAD-1** concentration had a minor effect on the *J*–*V* characteristics (Figure S37). The best EQE exclusive of emission from TPA-DCPP was 3.7% for the device containing 0.5 wt% **DAD-1** and 20 wt% TPA-DCPP. This value is comparable to those for the state-of-the-art TAF NIR-OLEDs[38] despite the solution-based device. The ideal EQE estimated from the PL quantum yield (Φ_{PL}) and light out-coupling efficiency based on the optical simulation was 7.1% (Figure S38). The ratio of the EQEs to the ideal ones decreased with increasing the **DAD-1** concentrations from approximately 0.5 for 0.5 wt% to 0.35 for 1.0 wt% and 0.28 for 1.5 wt% (Table S6). Considering similar career balances for all fabricated devices as anticipated from the above-mentioned small dependence of the *J*–*V* characteristics on the **DAD-1** concentrations, this result implies enhanced direct recombination on **DAD-1** molecules and attenuated contribution of the TAF mechanism in the high doping concentrations of **DAD-1**. Therefore, further improvement of the EQE may be possible by optimizing the TAF system in the future work.

Despite the increasing attention to the solid-state lasers with the successful electrical pumping and continuous wave operations in recent years, the number of organic NIR laser materials is still limited (Figure S39).[40,41] Therefore, the development of new NIR chromophores, which enables light amplification, is highly valuable.

The ASE threshold energy is inversely proportional to the stimulated emission cross-section (σ_{em}),[42] which is related to Einstein's *B* coefficient:

$$\sigma_{em}(\lambda) = \frac{h\nu n(\nu)}{c\Phi_{Fl}} BE_f(\nu) = \frac{\lambda^4 E_f(\lambda)}{8\pi n^2(\lambda) c\tau_{Fl}}$$

where λ is the wavelength, $E_f(\lambda)$ is the distribution of fluorescence quantum yield in wavelength, $n(\lambda)$ is the refractive index of the active gain layer, c is the speed of light, and τ_{Fl} is the fluorescence lifetime. This equation specifies that low Φ_{Fl} and long τ_{Fl} typical for most NIR emitters with strong CT natures make lasing difficult. In contrast, because of the high Φ_{Fl} and moderately short τ_{Fl} of **DAD-1**, a low ASE threshold was expected. In addition, the negligible excited state absorption at the emission wavelength is of great advantage.

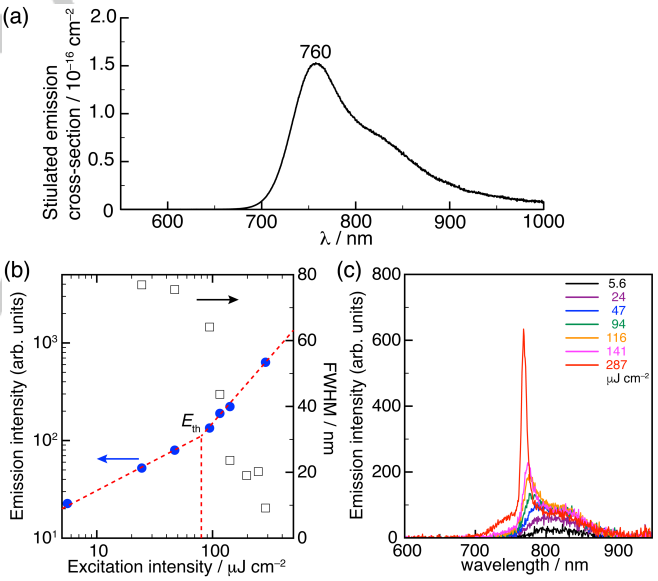

Figure 7. (a) Stimulated emission cross-section (σ_{em}) spectrum of **DAD-1** in a doped CBP film. (b) Output PL intensity (blue filled circle) and FWHM (black square) from the edge of **DAD-1**-doped CBP film as a function of excitation energy. (c) PL spectra of **DAD-1**-doped CBP film excited at different energies above and below the ASE threshold.

The ASE properties of **DAD-1** were investigated using a CBP film doped with 1 wt% **DAD-1** by optically pumping with a nitrogen laser at 337 nm (Figure 7 and Table S7). The σ_{em} of the dope film was estimated to be 1.5×10^{-16} at 760 nm, which is as high as those of organic lasing materials, such as bis(*N*-carbazolyl)styryl biphenyl (BSBCz).[43] Upon increasing the input intensity, the stimulated emission was observed at ca. 770 nm together with a

decrease of FWHM (Figure 7c). The ASE threshold energy of ca. 80 μJ cm^{-2} was determined from a change in the slope of emission as a function of input intensity (Figure 7b). According to a summary of materials and their ASE and lasing thresholds, which was reported by Kuehne and Gather[40] and replotted as a function of wavelength by us (Figure S39),[41] **DAD-1** is positioned in the NIR region with a sufficiently low ASE threshold, ensuring that PPABs are promising organic NIR laser materials.

Conclusion

In summary, the D–A–D architecture was successfully applied to shift the PPAB chromophores to the new fluorescence brightness range in the NIR region. The spacer units and heteroaromatic ring units played an important role in the control of D–A interactions to vary the intense emission from the HLCT state of **DAD-1** to the solvatochromic responses in emission due to the contribution of the CT state in the case of **DAD-2** and **DAD-3**. The HLCT state of **DAD-1** is ideal for redshifts of the emission to the NIR region without sacrificing the fluorescence brightness. Owing to the high Φ_{Fl}, the solution-processed NIR-OLED of **DAD-1** using the TAF system exhibited the high EQE of 3.7% at the EL maximum of ca. 760 nm. In addition, the high Φ_{Fl} and moderately short τ_{Fl} of **DAD-1** were also of benefit in achieving the low ASE threshold of ca. 80 μJ cm^{-2}. Overall, these results ensure high potential of PPAB as a NIR emitter in optoelectronic applications. Furthermore, considering the higher fluorescence brightness of the PPABs with benzothiazole and quinoline as a heteroaromatic ring unit (**Ph-2** and **Ph-3** in Figure 1) than that of **Ph-5** in the current study, there is a room to develop brighter and more redshifted NIR emitters by applying the D–A–D structure to these PPABs. Research along these directions will open new NIR materials science and practical applications.

Acknowledgements

This work was supported by Grants-in-Aid for Scientific Research (B) (JSPS KAKENHI Grant no. JP19H02703 and JP19H02790), Challenging Exploratory Research (JSPS KAKENHI Grant no. JP18K19081 and JP20K21227), Scientific Research on Innovative Areas, ‘‘π-System Figuration: Control of Electron and Structural Dynamism for Innovative Functions (no. 2601)’’ (JSPS KAKENHI Grant no. JP15H01001 and JP17H05160), the Murata Science Foundation, and JSPS Fellows (JSPS KAKENHI Grand no. JP19J12257). Y.K. thanks the Kyushu University Leading Program for “Molecular System for Devices” from MEXT, Japan. The work at Yonsei University was supported by the National Research Foundation of Korea (NRF) grant funded by the Korea government (MSIT) (No. 2020R1A5A1019141).

Conflict of interest

The authors declare no conflict of interest.

Keywords: amplified spontaneous emission • aza-BODIPY • NIR fluorescence • organic light emitting diode • transient absorption spectroscopy

[1] Z. Y. Wang, *Near-Infrared Organic Materials and Emerging Applications*; CRC Press: Florida, **2013**.
[2] W. Li, K. H. Hendriks, M. M. Wienk, R. A. J. Janssen, *Acc. Chem. Res.* **2016**, *49*, 78-85.
[3] A. Mishra, P. Bäuerle, *Angew. Chem.* **2012**, *124*, 2060-2109; *Angew. Chem. Int. Ed.* **2012**, *51*, 2020-2067.
[4] A. Zampetti, A. Minotto, F. Cacialli, *Adv. Funct. Mater.* **2019**, *29*, 1807623.
[5] P. A. Sullivan, L. R. Dalton, *Acc. Chem. Res.* **2010**, *43*, 10-18.
[6] L. Beverina, J. Fu, A. Leclercq, E. Zojer, P. Pacher, S. Barlow, E. W. Van Stryland, D. J. Hagan, J.-L. Brédas, S. R. Marder, *J. Am. Chem. Soc.* **2005**, *127*, 7282-7283.
[7] T.-L. Liu, S. Upadhyayula, D. E. Milkie, V. Singh, K. Wang, I. A. Swinburne, K. R. Mosaliganti, Z. M. Collins, T. W. Hiscock, J. Shea, A. Q. Kohrman, T. N. Medwig, D. Dambournet, R. Forster, B. Cunniff, Y. Ruan, H. Yashiro, S. Scholpp, E. M. Meyerowitz, D. Hockemeyer, D. G. Drubin, B. L. Martin, D. Q. Matus, M. Koyama, S. G. Megason, T. Kirchhausen, E. Betzig, *Science* **2018**, *360*, eaaq1392.
[8] G. Hong, A. L. Antaris, H. Dai, *Nat. Biomed. Eng.* **2017**, *1*, 0010.
[9] W. Fan, B. Yung, P. Huang, X. Chen, *Chem. Rev.* **2017**, *117*, 13566-13638.
[10] H. S. Jung, P. Verwilst, A. Sharma, J. Shin, J. L. Sessler, J. S. Kim, *Chem. Soc. Rev.* **2018**, *47*, 2280-2297.
[11] a) Y. Ge, D. F. O'Shea, *Chem. Soc. Rev.* **2016**, *45*, 3846-3864; b) J. Killoran, L. Allen, J. F. Gallagher, W. M. Gallagher, D. F. O'Shea, *Chem. Commun.* **2002**, *24*, 1862-1863.
[12] W. Zhao, E. M. Carreira, *Angew. Chem.* **2005**, *117*, 1705-1707; *Angew. Chem. Int. Ed.* **2005**, *44*, 1677-1679.
[13] V. F. Donyagina, S. Shimizu, N. Kobayashi, E. A. Lukyanets, *Tetrahedron Lett.* **2008**, *49*, 6152-6154.
[14] W. Sheng, Y. Wu, C. Yu, P. Bobadova-Parvanova, E. Hao, L. Jiao, *Org. Lett*. **2018**, *20*, 2620-2623.
[15] A. Loudet, K. Burgess, *Chem. Rev.* **2007**, *107*, 4891-4932.
[16] H. Lu, J. Mack, Y. Yang, Z. Shen, *Chem. Soc. Rev.* **2014**, *43*, 4778-4746.
[17] a) S. Shimizu, *Chem. Commun.* **2019**, *55*, 8722-8743; b) S. Shimizu, T. Iino, Y. Araki, N. Kobayashi, *Chem. Commun.* **2013**, *49*, 1621-1623; c) S. Shimizu, T. Iino, A. Saeki, S. Seki, N. Kobayashi, *Chem. Eur. J.* **2015**, *21*, 2893-2904.
[18] a) Y. Kage, H. Karasaki, S. Mori, H. Furuta, S. Shimizu, *ChemPlusChem.* **2019**, *84*, 1648-1652; b) Y. Kage, S. Mori, M. Ide, A. Saeki, H. Furuta, S. Shimizu, *Mater. Chem. Front.* **2017**, *2*, 112-120.
[19] R. Ishimatsu, H. Shintaku, Y. Kage, M. Kamioka, S. Shimizu, K. Nakano, H. Furuta, T. Imato, *J. Am. Chem. Soc.* **2019**, *141*, 11791-11795.
[20] a) R. Feng, N. Sato, M. Nomura, A. Saeki, H. Nakanotani, C. Adachi, T. Yasuda, H. Furuta, S. Shimizu, *J. Mater. Chem. C* **2020**, *8*, 8770-8776; b) R. Feng, N. Sato, T. Yasuda, H. Furuta, S. Shimizu, *Chem. Commun.* **2020**, *56*, 2975-2978.
[21] Li, L.; Wang, L.; Tang, H.; Cao, D. *Chem. Commun.* **2017**, *53*, 8352-8355.
[22] Y. Zhou, C. Ma, N. Gao, Q. Wang, P.-C. Lo, K. Wong, Q.-H. Xu, T. Kinoshita, D. K. P. Ng, *J. Mater. Chem. B* **2018**, *6*, 5570-5581.
[23] K. Miki, A. Enomoto, T. Inoue, T. Nabeshima, S. Saino, S. Shimizu, H. Matsuoka, K. Ohe, *Biomacromolecules* **2017**, *18*, 249-256.
[24] C. Wu, X. Huang, Y. Tang, W. Xiao, L. Sun, J. Shao, X. Dong, *Chem. Commun.* **2019**, *55*, 790-793.
[25] L. D. Lavis, R. T. Raines, *ACS Chem. Biol.* **2008**, *3*, 142-155.
[26] A. P. Gorka, R. R. Nani, M. J. Schnermann, *Org. Biomol. Chem.* **2015**, *13*, 7584-7598.
[27] Y.-C. Wei, S. F. Wang, Y. Hu, L.-S. Liao, D.-G. Chen, K.-H. Chang, C.-W. Wang, S.-H. Liu, W.-H. Chan, J.-L. Liao, W.-Y. Hung, T.-H. Wang, P.-T. Chen, H.-F. Hsu, Y. Chi, P.-T. Chou, *Nat. Photonics* **2020**, *14*, 570-577.
[28] F. Ding, Y. Zhan, X. Lu, Y. Sun, *Chem. Sci.* **2018**, *9*, 4370-4380.
[29] a) A. L. Antaris, H. Chen, K. Cheng, Y. Sun, G. Hong, C. Qu, S. Diao, Z. Deng, X. Hu, B. Zhang, X. Zhang, O. K. Yaghi, Z. R. Alamparambil, X. Hong, Z. Cheng, H. Dai, *Nat. Mater.* **2016**, *15*, 235-242; b) Q. Yang, Z. Hu, S. Zhu, R. Ma, H. Ma, Z. Ma, H. Wan, T. Zhu, Z. Jiang, W. Liu, L. Jiao, H. Sun, Y. Liang, H. Dai, *J. Am. Chem. Soc.* **2018**, *140*, 1715-1724.
[30] H. Ma, C. Liu, Z. Hu, P. Yu, X. Zhu, R. Ma, Z. Sun, C.-H. Zhang, H. Sun, S. Zhu, Y. Liang, *Chem. Mater.* **2020**, *32*, 2061-2069.

[31] K. Dhbaibi, L. Favereau, M. Srebro-Hooper, C. Quinton, N. Vanthuyne, L. Arrico, T. Roisnel, B. Jamoussi, C. Poriel, C. Cabanetos, J. Autschbach, J. Crassous, *Chem. Sci.* **2020**, *11*, 567-576.

[32] J. A. Carr, D. Franke, J. R. Caram, C. F. Perkinson, M. Saif, V. Askoxylakis, M. Datta, D. Fukumura, R. K. Jain, M. G. Bawendi, O. T. Bruns, *Proc. Natl. Acad. Sci. USA.* **2018**, *115*, 4465-4470.

[33] X. Peng, D. Draney, W. Volcheck, G. Bashford, D. Lamb, D. Grone, Y. Zhang, C. Johnson, *Proc. SPIE-Int. Soc. Opt. Eng. 6097E*, 1-12.

[34] a) W. Li, Y. Pan, L. Yao, H. Liu, S. Zhang, C. Wang, F. Shen, P. Lu, B. Yang, Y. Ma, *Adv. Opt. Mater.* **2014**, *2*, 892-901; b) W. Li, Y. Pan, R. Xiao, Q. Peng, S. Zhang, D. Ma, F. Li, F. Shen, Y. Wang, B. Yang, Y. Ma, *Adv. Funct. Mater.* **2014**, *24*, 1609-1614.

[35] a) M. E. El-Khouly, J. H. Kim, M. Kwak, C. S. Choi, O. Ito, K.-Y. Kay, *Bull. Chem. Soc. Jpn*. **2007**, *80*, 2465-2472; b) A. S. D. Sandanayaka, Y. Taguri, Y. Araki, T. Ishi-i, S. Mataka, O. Ito, *J. Phys. Chem. B* **2005**, *109*, 22502-22512.

[36] J. T. Buck, R. W. Wilson, T. Mani, *J. Phys. Chem. Lett.* **2019**, *10*, 3080-3086.

[37] D. Rehm, A. Weller, *Isr. J. Chem.* **1970**, *8*, 259-271.

[38] T. Yamanaka, H. Nakanotani, S. Hara, T. Hirohata, C. Adachi, *Appl. Phys. Express* **2017**, *10*, 074101.

[39] S. Wang, X. Yan, Z. Cheng, H. Zhang, Y. Liu, Y. Wang, *Angew. Chem.* **2015**, *127*, 13260-13264; *Angew. Chem. Int. Ed.* **2015**, *54*, 13068-13072.

[40] A. J. C. Kuehne, M. C. Gather, *Chem. Rev.* **2016**, *116*, 12823-12864.

[41] M. Mamada, T. Fukunaga, F. Bencheikh, A. S. D. Sandanayaka, C. Adachi, *Adv. Funct. Mater.* **2018**, *28*, 1802130.

[42] a) A. V. Deshpande, A. Beidoun, A. Penzkofer, G. Wagenblast, *Chem. Phys.* **1990**, *142*, 123-131; b) X. Liu, C. Py, Y. Tao, Y. Li, J. Ding, M. Day, *Appl. Phys. Lett.* **2004**, *84*, 2727-2729.

[43] T. Aimono, Y. Kawamura, K. Goushi, H. Yamamoto, H. Sasabe, C. Adachi, *Appl. Phys. Lett.* **2005**, *86*, 071110.

Entry for the Table of Contents

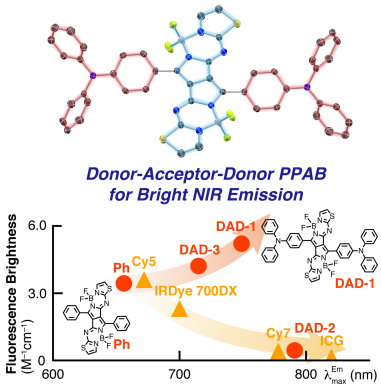

A bright NIR fluorescent molecule owing to the highly emissive hybridized locally excited and charge-transfer state was elaborated based on the donor–acceptor–donor (D–A–D) structure comprising an aza-BODIPY analog called PPAB as an acceptor. Its high external quantum efficiency of 3.7% and low amplified spontaneous emission threshold of ca. 80 μJ cm^{-2} in electroluminescence studies indicate the high potential for NIR optoelectronic applications.